Progress In Electromagnetics Research C, Vol. 131, 89–101, 2023

Yttria-Stabilized Zirconia Based Patch Antenna for Harsh Environment Applications

Aleks Mertvyy*, Md. S. I. Sagar, Noah Renk, Praveen Sekhar, and Tutku Karacolak

Abstract—Wireless devices that can operate under harsh environments are of great interest for military, space, and commercial applications such as antennas and radomes for fighter jets, wireless sensor networks for oil drilling and aircraft propulsion, and safety devices for first responders. Since antennas are key components of Radio Frequency (RF) Systems, it is crucial to have the antenna be able to withstand the same environmental hardships for a reliable and efficient communication. Various substrates have been utilized to implement antennas to withstand harsh environments and particularly high temperatures. Existing solutions such as silicon carbide (SiC), alumina, and polymer derived ceramics require complex deposition and patterning techniques, which make them unsuitable for low-cost RF and microwave applications. The main objective of this study is to explore microstrip patch antenna fabrication technology utilizing Zirconia Ribbon Ceramic (ZRC) materials and assess ZRC as a potential dielectric substrate for harsh environment applications. To do so, first, a wideband coplanar waveguide (CPW) fed monopole antenna is presented on a ZRC substrate operating within the S band. The proposed design has been manufactured using two separate methods including a clean room sputtering process and inkjet printing. A good agreement has been obtained between the measured results of the inkjet-printed prototype and simulations. Impedance matching and radiation patterns are investigated. The inkjet printing process has been shown to be a viable and cost-effective solution for fabricating ZRC-based patch antennas.

1. INTRODUCTION

Through various changes and advances in technology, there is a need to diversify the behavior of many devices and what they could be applied to. Concerning wireless devices, it is important to expand upon their capabilities and how they can be used in different environments. The specific environmental challenge that can be tackled by wireless devices is the presence of an ability to withstand harsh environments, particularly those that exhibit high temperatures. The availability of such devices would allow for multiple different applications that allow for exploration of hazardous and difficult locations. Some applications could include firefighting conditions that utilize wireless sensor networks [1], extreme environmental exploration such as volcanic and similar locations [2, 3], with additional possibilities that may include sensor deployment within space probes that may require a use of specialized antennas [4, 5]. Wireless devices utilize antennas, and it is important to have the antenna be able to withstand the same environmental hardships faced by the device that it is mounted on. In this context, the main objective of this study is to investigate utilization of a relatively new material for the role of dielectric substrate for microstrip patch antennas. This substrate is Zirconia Ribbon Ceramic (ZRC), a material based on Yttria-Stabilized Zirconia (YSZ) [6]. ZRC is a commercially available ceramic which has a great potential to be used in the design of functional devices due to its moisture resistant, high temperature

Received 1 February 2023, Accepted 10 March 2023, Scheduled 20 March 2023
* Corresponding author: Aleks Mertvyy (aleks.mertvyy@wsu.edu).
The authors are with the Department of Engineering and Computer Science, Washington State University Vancouver, Vancouver, WA 98686, USA.

tolerance, smooth surface, low thermal mass, mechanically robust, and abrasion resistant properties [7]. YSZ-based ceramics have been recently used in wide variety of gas sensing, biomedical, renewable energy, and thermal applications [8–12]. In [13], a silver-based square loop antenna on a zirconia substrate is presented to be used in biomedical implants for communication. Micro-wires have also been demonstrated in zirconia substrate for smart implant applications [14]. A dielectric helical antenna made of 3D-printed zirconia ceramic is proposed in [15]. It is shown that zirconia helical antenna possesses a lower radar cross section at high frequencies than conventional metal helical antennas. Similarly, in [16], a 3D printed zirconia dielectric resonator antenna using nanoparticle jetting is presented to characterize dielectric properties of zirconia material at microwave frequencies. Recently, an additively manufactured two-layer back-fed antenna is designed in [17] at 4.1 GHz using material jetting and microdispensing [18]. This work aims to explore YSZ-based microstrip patch antenna fabrication methods and assess antenna performance. The high dielectric constant and low loss tangent of YSZ make it an ideal candidate for realizing wireless systems with smaller electrical size and higher efficiency. Table 1 shows electrical and material properties of YSZ [19–21].

Table 1. YSZ substrate properties.

Attribute	Value
Relative Permittivity	23
Loss Tangent	0.001
Temperature Range	−200°C–1000°C
Thermal Conductivity	2.7 W/m-K
Electrical Resistivity	100 TΩ-cm

Possible areas of interest that could gain from the possibility of increase and improvements of existing high temperature substrates are those including the risk of high temperatures that are usually present in hazardous conditions. One job that involves constant risk in given conditions is that of firefighters. A few studies have been conducted within communications devices to be integrated within firefighter clothing. Consider similar types of possibilities for people that are involved in other types of study, as mentioned, for astronaut suits and other type of operational clothing [22–24]. These applications, however, limit their operation as more of a communication system, covering the possibilities that a firefighter may operate with during an immediate operation.

Further work on this topic, however, could be aimed to expand upon this by making a working antenna that can be attached to an unmanned sensor that studies an area of interest for dangerous gas presence or other hazardous wastes or presences. It could then be utilized to scout an area as necessary before sending people in to operate within. Of course, this would be important to have within an evacuated area for further area of interest exploration, where no lives are at risk, as can often be the case for firefighting applications. After this has been established, a number of sensors could be deployed in order to evaluate the area of interest and send data back in wireless signals to a control team [25]. The evaluated data would then be available as a way to organize the most effective strategy of approaching a given situation with limited risk to those approaching a situation.

With the necessary tools required for these situations under production, it is important to provide a possible antenna that could handle the difficulties under which the sensor is subject to. This would allow highly reduced failure due to the environment and maintain quality control in reporting accuracy of the sensor or sensor systems. Such antenna would have to be created with the ability to also perform on a substrate that has not been widely experimented or accepted as a usable patch antenna substrate. A recent study, however, was able to bring insight into similar behavior between high permittivity E-Strate substrate and commonly used substrate materials [20]. Through comparing antenna designs on various substrates for internet of things (IoT) applications, the study was able to demonstrate similar antenna performance obtained using an E-Strate substrate. Additionally, microstrip patch antennas using silicon carbide (SiC) material were proposed for high temperature and high power applications [26]. With a dielectric constant of 10, very narrow bandwidths were obtained at 10 GHz.

Through this experimentation, although it was proven that SiC was able to provide an operational antenna, there was no focus on expanding the possible bandwidth and improving impedance matching. Additional work done on substrates with a similar relative permittivity included a planar folded slot antenna on alumina substrate [27], which also had a focus on temperature dependency and its operation. Similarly, in [28, 29], a square slot antenna using alumina as the antenna substrate was presented as the interrogator antenna at X-band. Furthermore, aluminum nitride (AlN) antennas were studied in [30] for high-temperature sensor operations. Although these options are viable for the selected operation, with the permittivity being much higher within the ZRC, it may be more suitable for the fabrication of small form devices. Additionally, these substrates require clean room methods to fabricate which presents a more expensive option in antenna production [31]. ZRC, therefore, provides a strong alternative by being available as an antenna that can be fabricated through inkjet printing, making it a more affordable option for cheaper antenna fabrication.

In this study, our goal is to demonstrate the design and manufacturing of ZRC based microstrip patch antennas targeting harsh environment applications. To do so, a patch antenna is created in order to operate with a substantial bandwidth within the S-band frequency range. The proposed design includes a CPW-fed radiator and a ground plane which are both located on a single layer of ZRC substrate. Please note that the main aim of this study is not to design an S-band antenna with the best performance, but to present a compact antenna with wide bandwidth utilizing a ZRC substrate. This paper is an extension of the authors' previous work [32]. The study in [32] is based on only simulation results and does not present fabrication methods for ZRC based antennas. In addition to fabrication process, the current work presents measured results, design details including parametric study, and a detailed discussion on properties of ZRC material and antennas for harsh environment applications employing various substrates.

The following sections of this article will cover the design process through theory, simulations conducted, the fabrication of the antenna, testing and evaluation of the results that would serve to confirm or refute the plausible performance of this substrate within an antenna created for hazardous environments.

2. ANTENNA DESIGN

The antenna design process was covered in two steps that included the theoretical process and refinement through Ansys HFSS.

2.1. Theoretical Process for Initial Antenna Design

A ZRC substrate ($\epsilon_r = 23$, $\tan(\delta) = 0.001$) was utilized within the antenna design, with a standard provided size of 4×6 cm (40×60 mm) by High Tech Material Solutions (HTMS). The thickness of the available substrate, h, was at very thin 0.15 mm. Within these constraints, design goals are to implement a compact antenna and exhibit strong radiation at S band while maintaining a wide bandwidth. Additionally, coplanar waveguide (CPW) feeding has been selected due to its single metallic layer structure for simple fabrication and testing. CPW-feeding antennas have also been preferred to obtain wide bandwidth compared to other feeding structures.

Ansys HFSS is used to design and simulate the antenna. As shown in Figure 1, the proposed geometry has a CPW-fed rectangular patch and a partial ground plane on the top layer of the substrate. The width and length of the patch are initially found through the well-known process shown below as [33]:

$$W_p = \frac{v_o}{2f_r}\sqrt{\frac{2}{\epsilon_r + 1}} \tag{1}$$

where W_p is the width of the needed patch to achieve the desired resonant frequency, f_r, with the speed of light, v_o, and the electric permittivity, ϵ_r.

$$\epsilon_{reff} = \frac{\epsilon_r + 1}{2} + \frac{\epsilon_r - 1}{2}\sqrt{1 + \frac{12h}{W_p}} \tag{2}$$

The effective permittivity, ϵ_{reff}, is then found with the determined W_p, ϵ_r, and the given substrate height, h.

$$\frac{\Delta L_p}{h} = 0.412 \frac{(\epsilon + 0.3)\left(\frac{W_p}{h} + 0.264\right)}{(\epsilon - 0.258)\left(\frac{W_p}{h} + 0.8\right)} \tag{3}$$

The obtained variables, along with the given h, were then applied to Equation (3) in order to obtain the change in length, ΔL_p, which would find the effective electrical patch length, $L_{p,eff}$, of the antenna.

$$L_{p,eff} = L_p + 2\Delta L_p \tag{4}$$

In the final step, the length of the patch for the simulation would then be obtained through the relationship provided in Equation (4). The geometry of the initial design is then optimized through a parametric analysis to improve impedance matching and bandwidth in the band of operation.

2.2. Parametric Data Study and Antenna Refinement

The antenna design and refinement is conducted through the utilization of the optimetrics tool within ANSYS HFSS software. The dimensions of the radiator and ground plane are parameterized as shown in Figure 1. Design parameters with the greatest effect on the impedance matching and bandwidth are

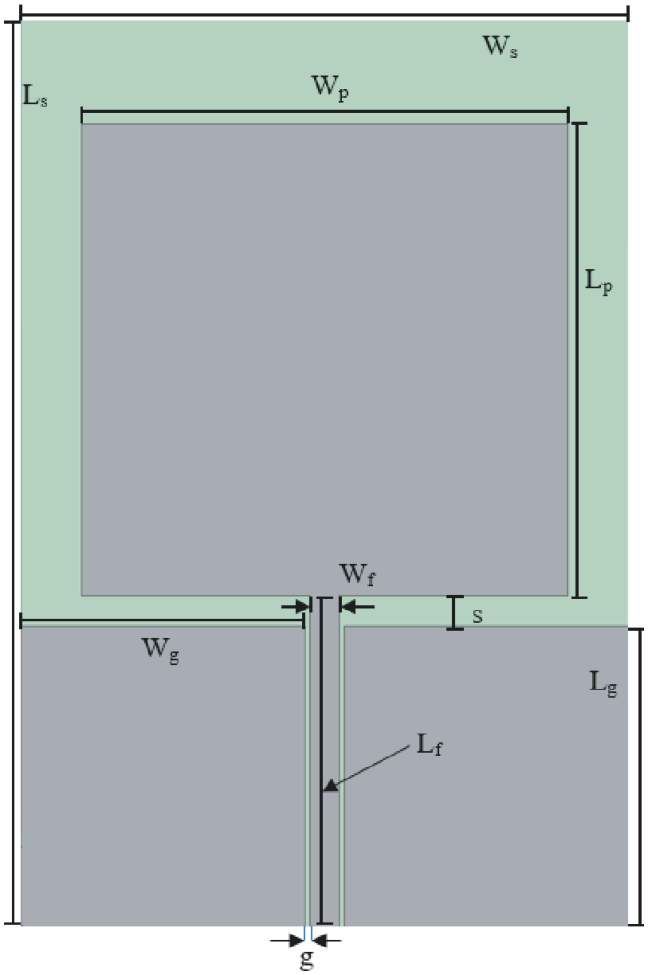

Figure 1. CPW-fed patch antenna with ZRC substrate.

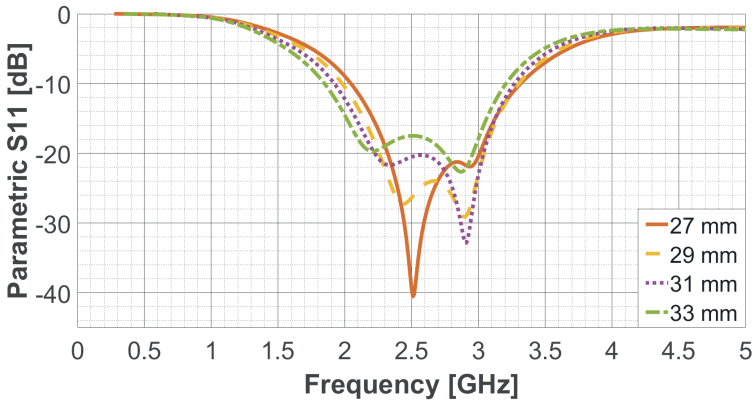

Figure 2. Patch Length Modifications with Patch Width at 32 mm.

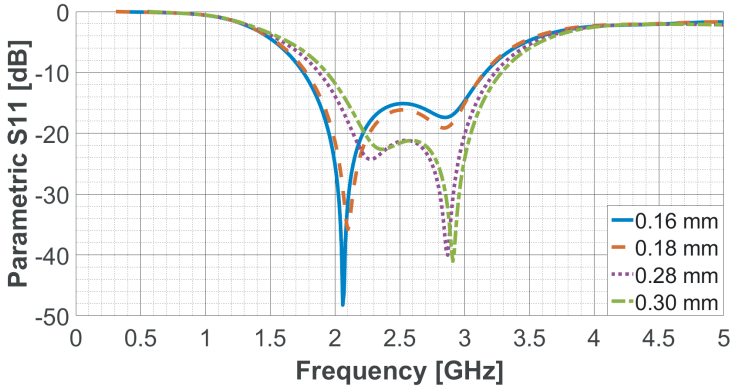

Figure 3. Gap width modification.

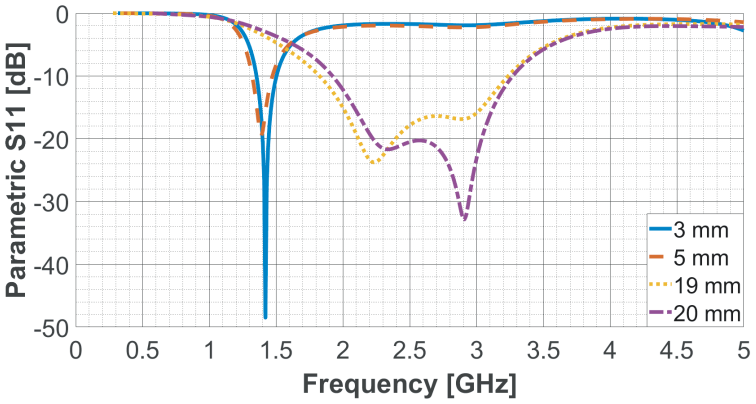

Figure 4. Ground length modification.

shown in Figures 2–5. It should be noted that during the parametric study, all dimensions are kept constant other than the tuned parameter.

Figures 2 and 3 give the return loss variation of the antenna while changing the length of the radiator and the gap between the feedline and the ground plane, respectively. As seen, both parameters affect impedance matching of the antenna over the S band. A patch length, L_p, of 31 mm and gap, g, of 0.3 mm are determined as the optimum dimensions. This is due to the balance between resonance strength and maximization of working range. Figure 2 demonstrates this balance by showing a choice

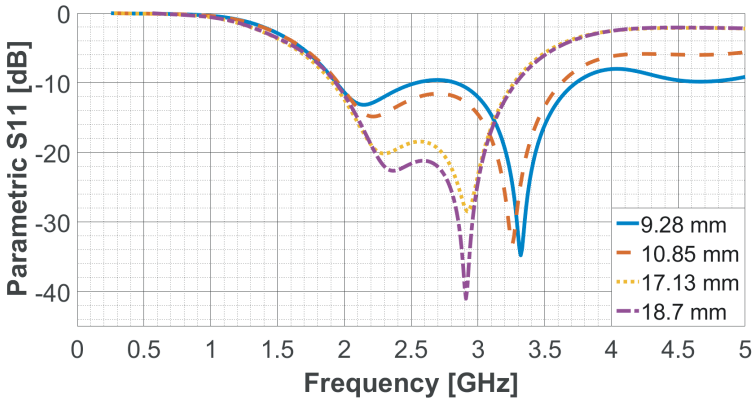

Figure 5. Ground width modifications.

made between stronger matching and an increase in the working range. Figure 3 further confirms this balance by showing a selection of higher-frequency return loss peak in selecting a gap. Similarly, ground plane dimensions contribute greatly to antenna performance as well. By making different changes to length and width of the ground plane, great changes in return loss can occur for this CPW antenna. As seen in Figures 4 and 5, a strong performance is obtained with ground plane length, L_g, and width, W_g, of 20 mm and 18.7 mm, respectively. The resulting optimized dimensions of the antenna are given in Table 2.

The optimized return loss for this antenna is presented in Figure 6. It is seen that the strongest resonance observed for this antenna is around 2.9 GHz. Additionally, there is another inverse peak at 2.34 GHz which shows a possible emerging second resonance within this antenna design. The antenna

Table 2. Dimensions of given CPW patch antenna.

Variable	Length (mm)	Variable	Length (mm)
L_s	60.0	W_s	40.0
L_p	31.0	W_p	32.0
L_f	22.0	W_f	2.0
L_g	20.0	W_g	18.7
s	2.0	g	0.3

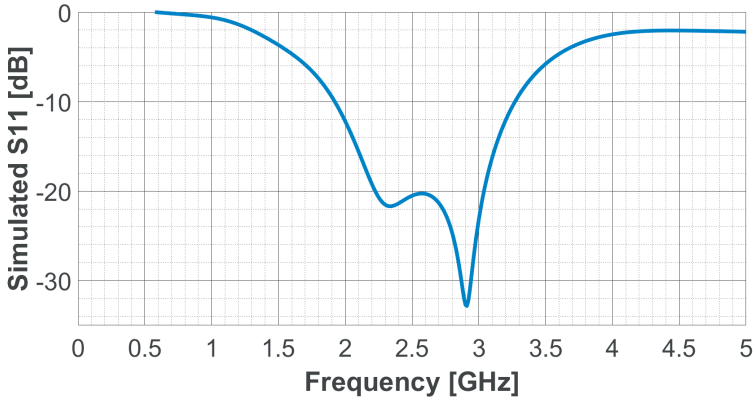

Figure 6. Simulated S_{11} of CPW-fed antenna.

has −10 dB impedance bandwidth of 52% covering frequencies from 1.92 GHz to 3.27 GHz (1.35 GHz, covering a substantial amount of S-Band frequencies), given the substrate thickness [34].

Additionally, the simulated peak gain is also obtained and provided in Figure 7. It can be seen that the peak gain is above 2 dB throughout the band while peaking at about 4 dB around the frequency of 3.2 GHz.

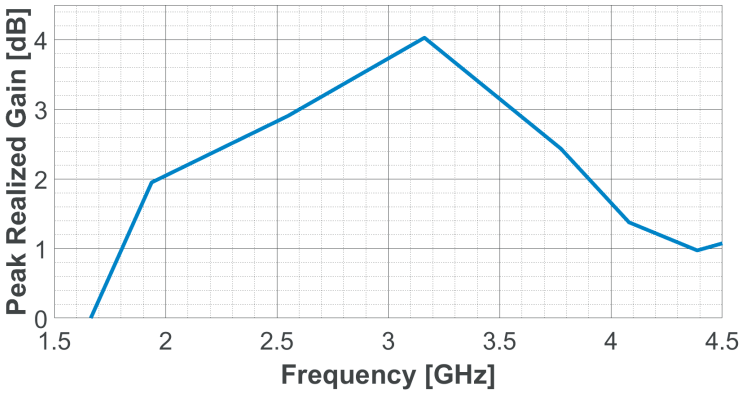

Figure 7. Simulated peak realized gain of CPW-fed antenna.

3. FABRICATION PROCESS

The fabrication of the antenna consisted of two processes. These are provided below.

3.1. Clean Room Sputtering Process

After considering various possibilities for working with the fabrication, first a sputtering process is introduced [35]. This would allow the usage of photolithography in order to apply the antenna design and then reveal the conductive design through sputtering, or metal deposition, utilizing lift-off as a final process to expose the antenna design. A complete process is conducted successfully, and the result is provided in Figure 8. The metal used for this process is aluminum, which has sufficient conductivity for testing, for which the simulation could be adjusted to accommodate.

Figure 8 shows the final results after the sputtering process. As can be observed within the images, the aluminum from the process is successfully applied to the antenna. The issue arose in the fact that

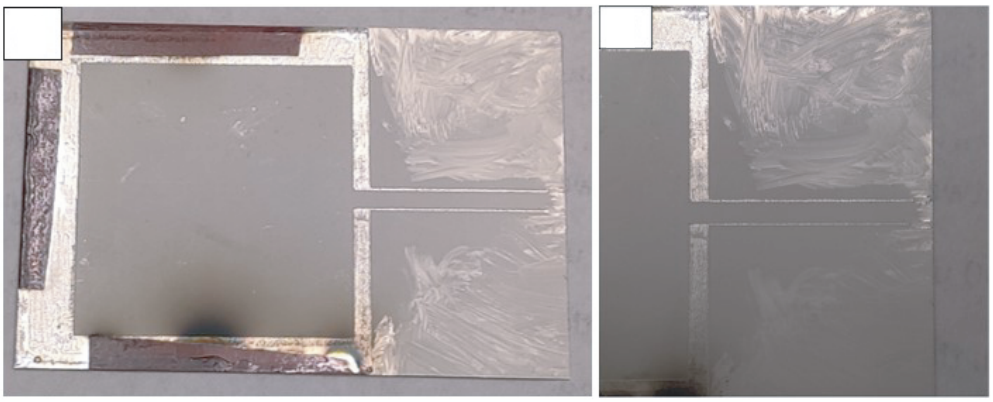

(a) (b)

Figure 8. Photolithography Results with (a) full antenna, (b) bottom half with feed line gaps.

the aluminum attached only to the areas covered by photoresist, which is removed at the end of this process by lift-off. The ZRC substrate exposing the antenna design itself did not retain the sputtered aluminum, proving the process to be unsuccessful in attaching aluminum to this ZRC substrate directly. The inability of this substrate to have direct attachment under this process would disqualify this process as a primary option (plainly applying conductive metals to the substrate) in future fabrications, as it introduces the necessity for sputtering layer techniques in order to successfully provide a working antenna design.

3.2. Inkjet Printer Model

After the unsuccessful sputtering test, an inkjet process is proposed in fabricating the antenna. The printing process is conducted utilizing the Dimatix Materials Printer (DMP-2831). A specialized cartridge is also used along with this printer, a Dimatix® Materials Cartridge (Samba® Cartridge). This cartridge is important due to its Native Drop Volume of 2.4 pL [36]. The printer itself is set up as presented below in Table 3.

Table 3. Printer setup specifications.

Parameter	Value	Unit
Drop Spacing	15	µm
Printed Layers	2	-
Sintering Temperature	110, 140	°C
Sintering Time	20, 30	min

The values presented in Table 3 show that the spacing between the drops is at its lowest available value with the number of layers selected for printing at 2, which allows the printer to perform the design application twice onto the substrate. The final process for the antenna to be complete is a double sintering process requiring the antenna to first be sintered at 110°C for 20 minutes, and then this process is repeated at 140°C for 30 minutes. The completion of this antenna is tested through a multimeter test in order to confirm conductivity of the patch, feed, and ground planes. The process is recorded and presented in Figure 9.

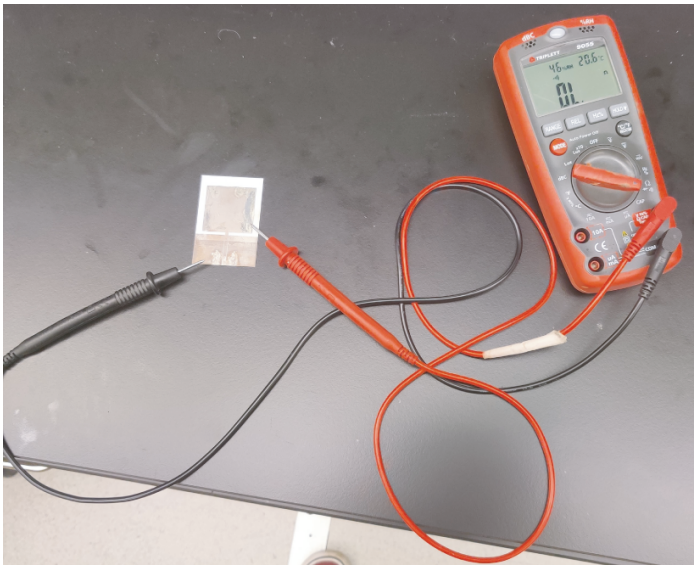

Figure 9. Setup for conductivity measurement.

The measurement is conducted by using the signal mode with resistance measurement, thus when the conductivity was present the sound would be made confirming that there is a short circuit for each individual printed ground and the patch and feed configuration. After the SMA connector is attached through soldering, supplemented by conductive paste, the test is conducted to confirm that there is a reliable connectivity between the feed line (and patch) and the SMA connector.

4. RESULTS AND DISCUSSION

The completed fabrication of the antenna is presented in Figure 10. From the antenna shown in Figure 10, it can be seen that the patch and ground planes were successfully recreated through the inkjet process. The image shows ground and feed line separation as well as a good shape for the patch of the antenna. One side of the patch is brushed with ink as a supplement of the printing process to cover any inconsistency. This is done in response to the completion process, following the sintering through which some conductive paste was altered or weakened. Afterwards, the conductivity is found to be solid throughout the full antenna print.

Figure 10. Antenna print with brushing.

The return loss (S_{11}) measurements of the fabricated antenna are performed using a Keysight FieldFox Microwave Analyzer N9952A and compared with simulated return loss. The measurement from the analyzer, as well as the simulated result, is available as a comparison of each other in Figure 11.

As seen, although there is a shift between the simulated and measured data, the results presented in Figure 11 serve to provide support for a viable antenna operating at normal conditions constructed on the ZRC substrate. The proposed antenna has simulated and measured -10 dB bandwidths of

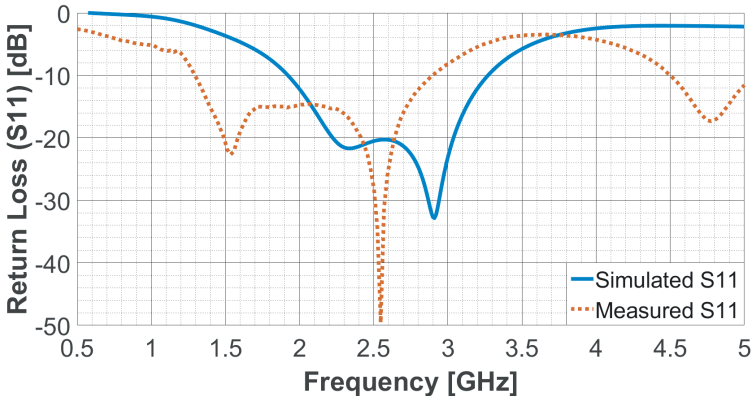

Figure 11. Simulated and measured results for antenna return loss (dB).

1.35 GHz (52%) and 1.6 GHz (77%), respectively. Both results confirm the antenna's ability to perform as a wideband antenna. The differences that appear in the comparison could be attributed to the imperfections of the fabrication materials as compared to theoretical possibility. Uneven ink layer distribution by the inkjet printer, losses and resistance matching from the SMA connector, and solder roughness may contribute to differences between the measured and simulated impedance matching.

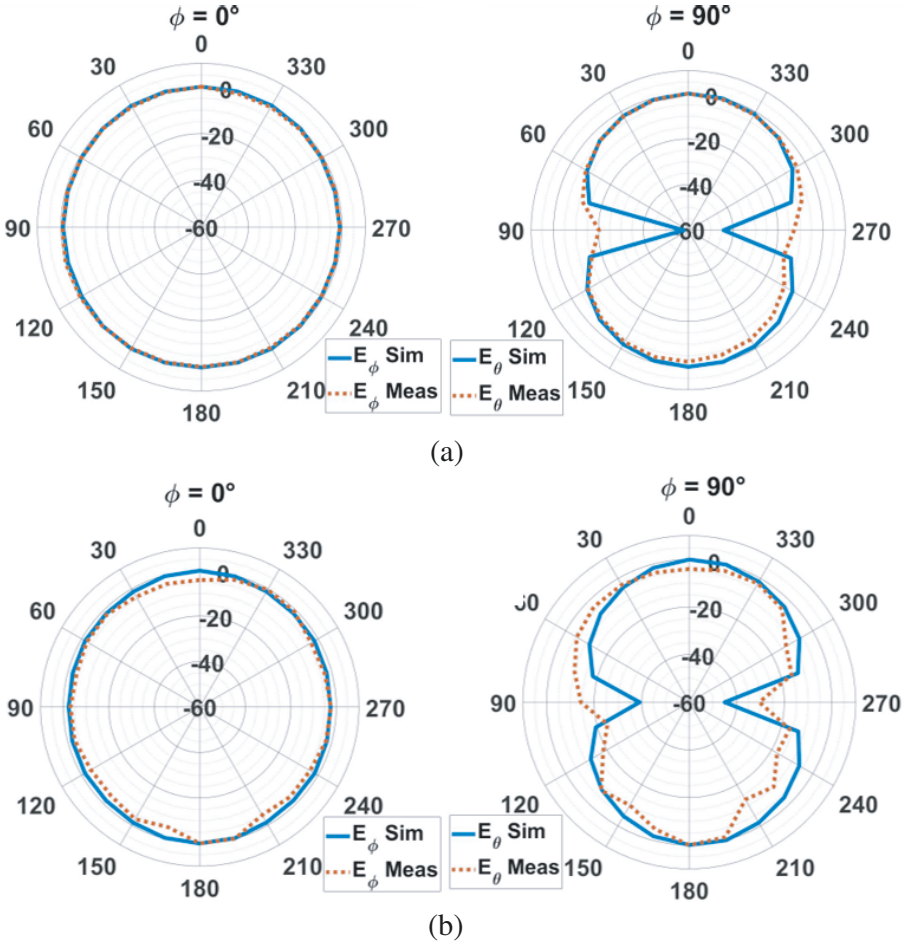

(a)

(b)

Figure 12. Measured and simulated radiation pattern of the antenna at (a) 2.3 GHz and (b) 2.5 GHz.

As a further comparison of operation, Figure 12 shows the simulated and measured radiation patterns for the antenna at 2.3 GHz and 2.5 GHz, respectively. A good agreement can be observed between the measured and simulated data for both x-z ($\phi = 0°$) and y-z ($\phi = 90°$) planes. As seen, the proposed antenna has a stable omnidirectional radiation pattern in the x-z plane and a dipole-like radiation pattern in the y-z plane for both frequencies within the band of operation.

For a more complete description of the radiation characteristics of the proposed antenna, the simulated 3D gain plots at 2.3 GHz and 2.5 GHz are also included in order to show the expected behavior of the antenna, due to its monopole structure and geometry. In Figure 13, it can be seen that both responses for the given frequencies exhibit strong behavior expected for a monopole antenna. There are no inconsistencies within the patterns with main beams stabilized in the broadside direction. Figure 13 also serves to show that the 3D gain patterns present gain values of 2.5 dB and 3.8 dB at 2.3 GHz and 2.5 GHz, respectively.

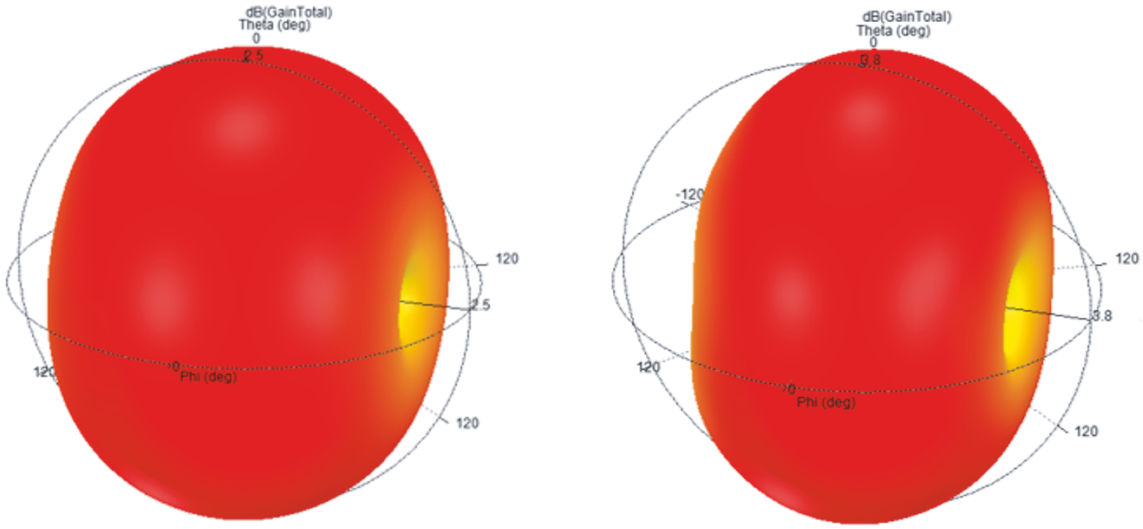

(a) (b)

Figure 13. Simulated 3D gain patterns for antenna at (a) 2.3 GHz and (b) 2.5 GHz.

5. CONCLUSION

In this paper, a patch antenna utilizing a ZRC substrate is presented as a possible tool to be used for various applications within high temperature environments. Through observation of the results, the antenna seems to operate convincingly within expected parameters. The trouble in applying aluminum through photolithography and metal deposition may prove problematic in future fabrication process. This, however, could be avoided through the inkjet printing process which has been proven viable in fabricating the antenna. The performance of the antenna confirms this fact by showing strong resonant behavior within a wide bandwidth and good radiation characteristics. Future work on this antenna would be conducted in order to open possibilities for further testing of the antenna within expected working conditions, including the expected high temperature conditions that it was made to withstand.

ACKNOWLEDGMENT

The authors acknowledge the input and help of Sam Judd in the photolithography and Aluminum (Al) deposition. Authors would like to thank Pulse Electronics for providing the necessary setup in anechoic chamber to measure antenna parameters. Authors also like to thank National Science Foundation (NSF) for supporting this work under Grant No. ECCS-2104513.

REFERENCES

1. Schubert, E. and S. Markus, "Evaluation of wireless sensor technologies in a firefighting environment," *Proceedings of International Conference on Networked Sensing Systems (INSS)*, IEEE Xplore, Kassel, Germany, June 15–18, 2010.
2. Werner-Allen, G., J. Johnson, M. Ruiz, J. Lees, and M. Welsh, "Monitoring volcanic eruptions with a wireless sensor network," *Proceedings of the Second European Workshop on Wireless Sensor Networks*, IEEE Xplore, Istanbul, Turkey, February 2, 2005.
3. Weng, F., H. Yang, and X. Zou, "On convertibility from antenna to sensor brightness temperature for ATMs," *IEEE Geoscience and Remote Sensing Letters*, Vol. 10, No. 4, 771–775, 2013.
4. Bangert, J. T., R. S. Engelbrecht, E. T. Harkless, R. V. Sperry, and E. J. Walsh, "The spacecraft antennas," *The Bell System Technical Journal*, Vol. 42, No. 4, 869–897, 1963.
5. Bittner, D., A. Cody, C. Eubank, C. Jorgensen, T. Reppert, J. Shultis, B. Streetman, and D. Ziegler, "Follow-on mission for the hubble space telescope," 2004.
6. Specifications, "SZ0429 Yttria stabilized Zirconia Y_2O_3*ZrO_2 (YSZ)," *Stanford Advanced Materials*, [Online], Available: https://www.samaterials.com/zirconium/429-yttria-stabilized-zirconia.html.
7. Aryal, M., S. W. Allison, K. Olenick, and F. Sabri, "Flexible thin film ceramics for high temperature thermal sensing applications," *Optical Materials*, Vol. 100, 109656, 2020.
8. Koo, J. Y., Y. Lim, Y. B. Kim, D. Byun, and W. Lee, "Electrospun yttria-stabilized zirconia nanofibers for low-temperature solid oxide fuel cells," *International Journal of Hydrogen Energy*, Vol. 42, No. 24, 15903–15907, 2017.
9. Soon, G., B. Pingguan-Murphy, and S. A. Akbar, "Modulation of osteoblast behavior on nanopatterned yttria-stabilized zirconia surfaces," *Journal of the Mechanical Behavior of Biomedical Materials*, Vol. 68, 26–31, 2017.
10. López-Gándara, C., F. M. Ramos, and A. Cirera, "YSZ-based oxygen sensors and the use of nanomaterials: A review from classical models to current trends," *Journal of Sensors*, Vol. 2009, 1–15, 2009.
11. Skinner, S. J., J. P. Feist, I. J. E. Brooks, S. Seefeldt, and A. L. Heyes, "YAG: YSZ composites as potential thermographic phosphors for high temperature sensor applications," *Sensors and Actuators B: Chemical*, Vol. 136, No. 1, 52–59, 2009.
12. Zhu, Y., K. Liu, J. Deng, J. Ye, F. Ai, H. Ouyang, T. Wu, J. Jia, X. Cheng, and X. Wang, "3D printed zirconia ceramic hip joint with precise structure and broad-spectrum antibacterial properties," *Int. J. Nanomed.*, Vol. 14, 5977–5987, 2019.
13. Moura, C. G., H. Dinis, O. Carvalho, P. M. Mendes, R. M. Nascimento, and F. S. Silva, "A novel approach for micro-antenna fabrication on ZrO_2 substrate assisted by laser printing for smart implants," *Applied Sciences*, Vol. 12, 9333, 2022.
14. Moura, C. G., D. Faria, O. Carvalho, R. Pereira, M. Cerqueira, R. Nascimento, and F. S. Silva, "Laser printing of silver-based micro-wires in ZrO_2 substrate for smart implant applications," *Optics & Laser Technology*, Vol. 131, 106416, 2020.
15. Wang, S., L. Zhu, Y. Li, G. Zhang, J. Yang, J. Wang, and W. Wu, "Radar cross-section reduction of helical antenna by replacing metal with 3-D printed zirconia ceramic," *IEEE Antennas and Wireless Propagation Letters*, Vol. 19, No. 2, 350–354, 2020.
16. Oh, Y., V. Bharambe, B. Mummareddy, J. Martin, J. McKnight, M. A. Abraham, J. M. Walker, K. Rogers, B. Conner, P. Cortes, E. MacDonald, and J. J. Adams, "Microwave dielectric properties of zirconia fabricated using nanoparticle jetting," *Additive Manufacturing*, Vol. 27, 586–594, 2019.
17. Mejias-Morillo, C. R., J. B. Shivakumar, S. L. Yu, B. Roberts, P. Cortes, E. Macdonald, A. V. Polotai, and E. A. Rojas-Nastrucci, "High-temperature additively manufactured C-band antennas using material jetting of zirconia and micro-dispending of platinum paste," *IEEE Open Journal of Antennas and Propagation*, Vol. 3, 1289–1301, 2022.
18. Mummareddy, B., D. Negro, V. T. Bharambe, Y. Oh, E. Burden, M. Ahlfors, J. Choi, A. D. Plessis, J. Adams, E. Macdonald, and P. Cortes, "Mechanical properties of material jetted zirconia complex

geometries with hot isostatic pressing," *Advances in Industrial and Manufacturing Engineering*, Vol. 3, 100052, 2021.

19. Harrop, P. J. and J. N. Wanklyn, "The dielectric constant of zirconia," *British Journal of Applied Physics*, Vol. 18, 739, 1967
20. Elena de Cos Gomez, M., H. Fernandez Alvarez, B. Puerto Valcarce, C. Garcia Gonzalez, J. Olenick, and F. Las-Heras Andres, "Zirconia-based ultra-thin compact flexible CPW-fed slot antenna for IoT," *Micromachines*, Vol. 19, No. 14, 3134, 2019.
21. Datasheet, "ENrG thin E-strate®, Zirconia Ribbon Ceramic Substrate," *MatWeb: Material Property Data*, [Online], Available: https://www.matweb.com/search/datasheet.aspxmatguid=7a3cd87004934e1f83f0fd7f34813948& ckck=1.
22. Hertleer, C., H. Rogier, L. Vallozzi, and L. Van Langenhove, "A textile antenna for off-body communication integrated into protective clothing for firefighters," *IEEE Transactions on Antennas and Propagation*, Vol. 57, No. 4, 919–925, 2009.
23. Vanveerdeghem, P., H. Rogier, J. Knockaert, P. Van Torre, and C. Stevens, "Flexible dual-diversity wearable wireless mode integrated on dual-polarised textile patch antenna," *IET Science, Measurement & Technology*, Vol. 8, No. 6, 452–458, 2014.
24. Declercq, F., A. Georgiadis, and H. Rogier, "Wearable aperture-coupled shorted solar patch antenna for remote tracking and monitoring applications," *Proceedings of the 5th European Conference on Antennas and Propagation (EUCAP)*, IEEE Xplore, Rome, Italy, May 31, 2011.
25. Rhys Le Comte, B., G. Sen Gupta, and M. Tin Chew, "Distributed sensors for hazard detection in an urban search and rescue operation," *2012 IEEE International Instrumentation and Measurement Technology Conference Proceedings*, IEEE Xplore, Graz, Austria, July 2, 2012.
26. Karacolak, T., R. V. K. Thirmulai, J. Neil Merrett, Y. Koshka, and E. Topsakal, "Silicon Carbide (SiC) antennas for high-temperature and high-power applications," *IEEE Antennas and Wireless Propagation Letters*, Vol. 12, 409–412, 2013.
27. Scardelletti, M. C., J. L. Jordan, and G. E. Ponchak, "Temperature dependency (25°C–400°C) of a planar folded slot antenna on alumina substrate," *IEEE Antenna and Wireless Propagation Letters*, Vol. 7, 489–492, 2008.
28. Cheng, H., X. Ren, S. Ebadi, and X. Gong, "A wide-band square slot antenna for high-temperature applications," *Proceedings IEEE APS/URSI International Symposium*, IEEE Xplore, Orlando, Florida, January 27, 2014.
29. Cheng, H., X. Ren, S. Ebadi, Y. Chen, L. An, and X. Gong, "Wireless passive temperature sensors using integrated cylindrical resonator/antenna for harsh-environment applications," *IEEE Sensors Journal*, Vol. 15, No. 3, 1453–1462, 2014.
30. Yan, D., Y. Yang, Y. Hong, T. Liang, Z. Yao, X. Chen, and J. Xiong, "AlN-based ceramic patch antenna-type wireless passive high-temperature sensor," *Micromachines*, Vol. 8, No. 10, 301, 2017.
31. Zhu, D., "Aerospace ceramic materials: Thermal, environmental barrier coatings and SiC/SiC ceramic matrix composites for turbine engine applications," *Nat. Aeronaut. Space Admin.*, NASA/TM-2018-219884, 2018.
32. Mertvyy, A., N. Renk, V. Bigelow, B. A. Younes, P. Sekhar, and T. Karacolak, "A wideband CPW-fed monopole antenna for high-temperature applications," *Proceedings IEEE APS/URSI International Symposium*, IEEE Xplore, Denver, Colorado, July 10–15, 2022.
33. Balanis, C. A., *Antenna Theory: Analysis and Design*, 4th Edition, John Wiley & Sons, Inc., Hoboken, New Jersey, 2016.
34. Pozar, D. M., "Microstrip antennas," *Proceedings of the IEEE*, Vol. 80, No. 1, 79–91, 1992.
35. Depla, D., S. Mahieu, and J. E. Greene, *Sputter Deposition Processes*, 253–296, William Andrew Applied Science Publishers, 2009.
36. FUJIFILM Specification Sheet, "Dimatix® Materials Cartridge — Samba® Cartridge," *FUJIFILM Dimatix*, [Online], Available: https://f.hubspotusercontent30.net/hubfs/5352080/Samba%20Cartridge.pdf.